

THE HUBBLE SPACE TELESCOPE SAMPLE OF RADIO-LOUD QUASARS: THE $\text{Ly}\alpha/\text{H}\beta$ RATIO¹

HAGAI NETZER,² M. S. BROTHERTON,³ BEVERLEY J. WILLS,³ MINGSHENG HAN,^{3,4} D. WILLS,³ J. A. BALDWIN,⁵
 G. J. FERLAND,⁶ AND I. W. A. BROWNE⁷

Received 1994 July 25; accepted 1995 January 19

ABSTRACT

We have used the first *Hubble Space Telescope* Faint Object Spectrograph spectra of our sample of radio-loud quasars, and quasi-simultaneous ground-based spectrophotometry, to investigate the intensity ratio $\text{Ly}\alpha/\text{H}\beta$, whose small observed values are one of the outstanding problems of active galactic nuclei research. The present sample of 20 quasars with complete flux and profile data shows the first significant correlations of this ratio with other observed properties. The strongest correlations are with various continuum slope indicators: we find smaller $\text{Ly}\alpha/\text{H}\beta$ ratios in quasars whose continua rise more steeply into the red. The long-wavelength continuum slope (1909–4861 Å) is strongly correlated with $\text{Ly}\alpha/\text{H}\beta$, but the short-wavelength continuum slope (1215–1909 Å) is not. A separation into line components shows that the above correlations arise mostly from the red wings of the lines. The core-to-wing flux ratio is also correlated with the slope. The correlation of $\text{Ly}\alpha/\text{H}\beta$ with continuum slope is consistent with line and continuum reddening by an external dust screen with Galactic-type extinction of up to $E_{B-V} = 0.3$. In this case the intrinsic $\text{Ly}\alpha/\text{H}\beta$ ratio is ~ 20 . However, other trends expected if dust were the sole factor are not seen. There are indications that core-dominated and lobe-dominated sources differ in their $\text{Ly}\alpha/\text{H}\beta$ and continuum slope dependence. We calculate a grid of theoretical hydrogen line ratios and use it to investigate reddening and alternative explanations, such as dependence upon ionizing flux. We suggest that several different mechanisms are operating.

Subject headings: galaxies: active — line: profiles — quasars: emission lines — quasars: general — radio continuum: galaxies — ultraviolet: galaxies

1. INTRODUCTION

One of the outstanding problems of active galactic nuclei (AGNs) research is the unusually small observed $\text{Ly}\alpha/\text{H}\beta$ intensity ratio (typically 5–15) in the broad-line region (BLR) spectrum compared with the prediction of simple recombination theory (30–50). This problem was first noted by Baldwin (1977) and was extensively discussed observationally (Puetter et al. 1981; Soifer et al. 1981; Allen et al. 1982; Wu, Boggess, & Gull 1983; Kriss 1984, 1986) and theoretically (Netzer & Davidson 1979; Kwan & Krolik 1981; Canfield & Puetter 1981; Puetter et al. 1981; Weisheit, Shields, & Tarter 1981; Collin-Souffrin et al. 1981, 1986; Ferland & Mushotzky 1982; Kriss 1984; Kwan 1984, 1986; Hubbard & Puetter 1984; Wills, Netzer, & Wills 1985; Kallman & Krolik 1986; Collin-Souffrin & Dumont 1989; Avrett & Loeser 1988; Rees, Netzer, & Ferland 1989; Ferland & Persson 1989; see Netzer 1990 for a review).

A major problem in understanding the observed $\text{Ly}\alpha/\text{H}\beta$ ratio is the lack of a theoretical model involving a complete treatment of line formation and radiative transfer (see the discussion in § 4 below). Present-day models are quite complete in their treatment of atomic processes at the expense of an approximate approach to the line transfer problem. It would help if correlations between the observed $\text{Ly}\alpha/\text{H}\beta$ ratio and other known properties of AGNs could be found. But no sufficiently large data sets have been available with accurate and simultaneous $\text{Ly}\alpha$ and $\text{H}\beta$ observations.

We have undertaken a program of observation with the *Hubble Space Telescope* (*HST*) to investigate this, and other questions about radio-loud quasars. Our sample was chosen to study the dependence of UV-optical spectral properties on orientation of the axis of the central engine. Thus we include a wide range of the ratio, R , of radio core luminosity (supposedly beamed) to radio lobe luminosity (supposedly isotropic). In order to isolate possible orientation effects from those dependent on intrinsic luminosity, we have selected objects on the basis of their lobe luminosity. If core emission is not predominantly beamed, then we are investigating dependences on intrinsic core luminosity. We started with the QSOs in the 3CR catalog, and then added core-dominated sources of similar redshift and extended radio luminosity. Further details are given in two earlier papers: Wills et al. (1993, an investigation of the narrow emission lines, hereafter Paper I) and Wills et al. (1995a, a description of our *HST*/Faint Object spectrograph [FOS] data for 31 quasars, hereafter Paper II).

We have made a considerable effort to secure simultaneous ground-based data, covering, in almost all cases, the entire 1100–5200 Å rest-wavelength range. As well as the wide wavelength coverage, our low-redshift sample has the advantage that the $\text{Ly}\alpha$ profile is not significantly affected by intergalactic

¹ Based on observations with the NASA/ESA *Hubble Space Telescope*, obtained at the Space Telescope Science Institute, which is operated by the Association of Universities for Research in Astronomy, Inc., under NASA contract NAS 5-26555.

² School of Physics and Astronomy, Raymond and Beverly Sackler Faculty of Exact Sciences, Tel Aviv University, Tel Aviv 69978, Israel.

³ McDonald Observatory and Department of Astronomy, University of Texas at Austin, Austin, TX 78712.

⁴ Now at Department of Astronomy, University of Wisconsin, Madison, WI 53706.

⁵ Cerro Tololo Inter-American Observatory, National Optical Astronomy Observatories, P.O. Box 26732, Tucson, AZ 85726. Operated by AURA, Inc., under cooperative agreement with the National Science Foundation.

⁶ Department of Physics and Astronomy, University of Kentucky, Lexington, KY 40506-0055.

⁷ University of Manchester Nuffield Radio Astronomy Laboratories, Jodrell Bank, Macclesfield, Cheshire, SK11 9DL, England.

absorption lines. The ground-based data for the 31 objects, as well as a detailed discussion of line profile, line intensity, and continuum correlations, will be given in a forthcoming paper (Wills et al. 1995b).

The present paper is based on a partial data set containing 20 quasars with flux and profile information on both $\text{Ly}\alpha$ and $\text{H}\beta$. We are thus in a position to investigate the $\text{Ly}\alpha/\text{H}\beta$ ratio, as well as several other properties, in a way never attempted before. Section 2 below gives information about the observations and data reduction pertaining to this sample. In § 3 we show the first ever observed statistically significant correlations of the $\text{Ly}\alpha/\text{H}\beta$ ratio with other properties and discuss some known and expected trends. Section 4 includes a discussion of the new correlations, including new theoretical calculations, and the possible implications for the physical conditions in high-luminosity AGNs.

2. OBSERVATIONS

2.1. *HST* Observations

A detailed description of the *HST*/FOS observations is given in Paper II. Below is a summary pertaining to the present study.

HST/FOS observations were obtained for all sources in our sample with $z < 1.8$ and $V < 18$. We have used the various FOS grating settings to cover the spectral region from below $\text{Ly}\alpha$ to observed wavelengths of 3250 or 4800 Å, with $\text{S/N} \approx 22$ per diode, in the continuum. The effective spectral resolution corresponds to $\sim 350 \text{ km s}^{-1}$ and the photometric accuracy, given the 4.3×4.3 aperture used, is $\sim 5\%$. Wavelength determination is crucial for the present work. We have used the $[\text{O III}] \lambda 5007$ line to determine the redshift and the internal FOS calibration to obtain UV wavelengths. In some cases, we could check the *HST* wavelength scale using Galactic interstellar lines. The accuracy of the wavelength scale is $\sim 100 \text{ km s}^{-1}$ with a few exceptions of 200–300 km s^{-1} . Paper II gives line intensity and other information not listed here, and Figure 1 shows the continuum-subtracted $\text{Ly}\alpha$ region for all 20 objects used in this work. Objects are identified by the first four digits of the coordinate name, or by the full coordinate name in cases of ambiguity.

2.2. Ground-based Observations

We attempted to obtain data from the atmospheric cutoff near 3200 Å to beyond $\text{H}\beta$ or $\text{H}\alpha$ within a few days of the *HST* observations, or within a day for the most variable quasars, but such quasi-simultaneous observations were not always possible. The optical region between 3200 Å and $1 \mu\text{m}$ was observed from McDonald Observatory (2.7 m), Kitt Peak National Observatory (KPNO; 2.1 m), or Cerro Tololo Inter-American Observatory (CTIO; 4 m). Near-infrared spectra were observed with the 4 m United Kingdom Infrared Telescope (UKIRT). Details of the ground-based observations, including observing logs and specific information on individual objects, are given by Wills et al. 1995b).

Most data in the $\text{H}\beta$ - $[\text{O III}] \lambda 5007$ region were obtained at McDonald with a significant number also from KPNO and CTIO. Short exposures with a large projected slit width of typically 8" were made for spectrophotometry, and longer exposures with an $\sim 2''$ slit were made for best S/N 's and wavelength resolution equivalent to ~ 350 – 600 km s^{-1} . For a subset of objects, these were supplemented by McDonald observations of higher resolution (200–300 km s^{-1}) made

for a parallel investigation of the $\text{H}\beta$ - $[\text{O III}] \lambda 5007$ profiles (Brotherton 1995). Telluric absorption bands were removed using spectra of hot stars observed close to the QSOs in time and air mass.

All optical spectra were reduced using the NOAO package within IRAF. The estimated absolute flux calibration uncertainties are $\sim 5\%$. Wavelength scales were checked both internally, using multiple exposures and sky lines, and externally by comparing narrow lines in the McDonald spectra with those from KPNO's Goldcam spectrograph. The internal consistency of the wavelength scale was a few tenths of an angstrom (rms), with an estimated absolute error of less than 1 Å.

For PKS 0859–14 and DA 406, $\text{H}\beta$ falls in the *J* band and the data were obtained with the CGS4 spectrometer on UKIRT. The resolution (FWHM) was $\sim 1000 \text{ km s}^{-1}$ and spectral coverage was $51,000 \text{ km s}^{-1}$.

Figure 2 shows the 20 continuum-subtracted $\text{H}\beta$ profiles used here. Note that the Fe II blends (see § 3.1) and the narrow $[\text{O III}]$ lines have been subtracted, but the narrow $\text{H}\beta$ core is shown.

3. RESULTS

3.1. *New Line and Continuum Measurements*

Our optical and UV data sets were processed in several stages to obtain the $\text{Ly}\alpha/\text{H}\beta$ line ratio and the continuum shape. First, we applied a correction for reddening in our galaxy, as described in Paper II. At short observed wavelengths the uncertainties in this correction can be significant. Fortunately, the uncertainties become less at the longer, redshifted wavelengths. For our sample, typical uncertainties are 5%, with a few up to 8%. The exception is 0710+118 (3C 175) with an uncertainty of 15%. Then we proceeded to isolate $\text{Ly}\alpha$ profiles. The procedure involves setting the local underlying continuum and decomposing the $\text{Ly}\alpha$ and N V $\lambda 1240$ blend into several Gaussian components. This was achieved using GAUSSFIT or the various procedures supplied in IRAF. The best fits thus obtained were used to remove the N V $\lambda 1240$ line and to recover the $\text{Ly}\alpha$ profiles over wavelength ranges affected by absorption. We are thus left with smooth, absorption-free $\text{Ly}\alpha$ profile fits.

In the case of $\text{H}\beta$ we have removed a narrow Gaussian component constrained to have the same width as the $[\text{O III}] \lambda 5007$ line. The Fe II blends were removed using the empirical model derived by Boroson & Green (1992) from the spectrum of I Zw 1 (PG 0050+124), a low-luminosity QSO with "narrow" broad lines and strong Fe II emission. For each spectrum, this model was broadened by convolution with a Gaussian profile of constant velocity width and scaled by a multiplicative factor, to fit the broad Fe II features at 4450–4700 and 5150–5350 Å. The subtraction of this model removes Fe II from under the $\text{H}\beta$ and $[\text{O III}] \lambda 5007$ profiles. We have estimated the local continuum by linear interpolation and fitted the "cleaned" broad $\text{H}\beta$ profile with up to three Gaussian components (except for one object, 0903, where 10 components have been used). This procedure is a way of smoothing the profiles and is not meant to indicate a preference for a particular theoretical shape or a cloud kinematic model.

In the rest of the discussion we consider only broad hydrogen lines and the continuum. These are spatially unresolved and so completely included within our projected aperture sizes. This is also the case for the dusty obscurer considered below.

Figure 3 shows normalized $\text{Ly}\alpha$ and $\text{H}\beta$ profiles for the 20

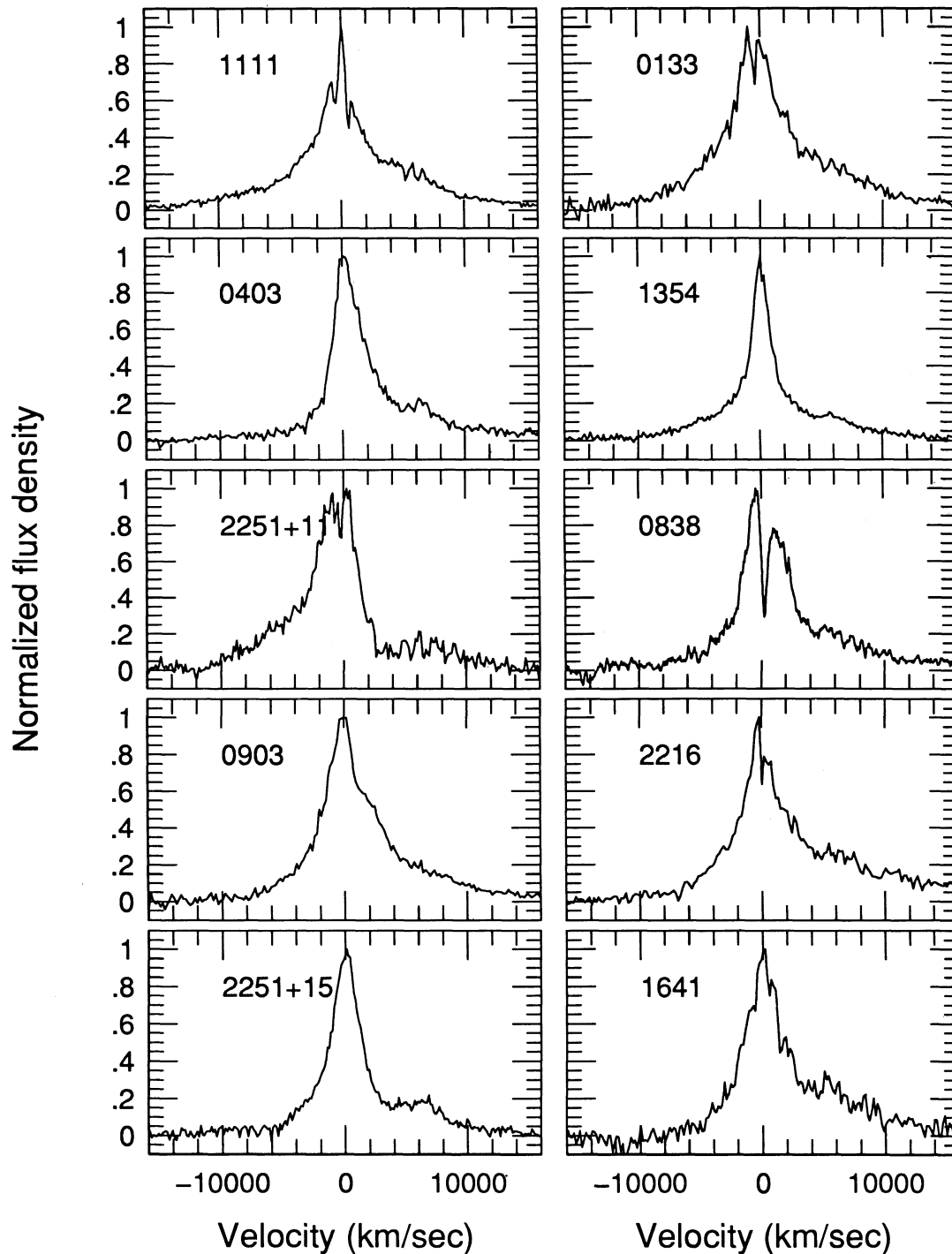


FIG. 1.—Continuum-subtracted, normalized Ly α profiles for the 20 radio-loud quasars discussed in this work

objects discussed in this work. The objects are arranged in order of increasing UV-optical spectral index $\alpha_{4861-1215}$ (see below), and the zero of the velocity scale is determined from the narrow [O III] $\lambda 5007$ line.

Flux measurements were performed on all the Ly α and H β lines using the deblended, continuum-subtracted profiles. This enables us to form the ratio of H β /Ly α as a function of velocity which we also plot in Figure 3. We draw attention to the fact that for several objects this ratio approaches, and even exceeds,

unity in the wings of the lines. This is something we will discuss further in § 4. In order to try and quantify these changes of line ratio with velocity in a way in which we can search for correlations with other parameters, we subdivided the lines into components in three ways:

1. Two components, blue and red, divided at zero velocity as determined by the [O III] $\lambda 5007$ line redshift.
2. Three components, a blue wing, a core, and a red wing,

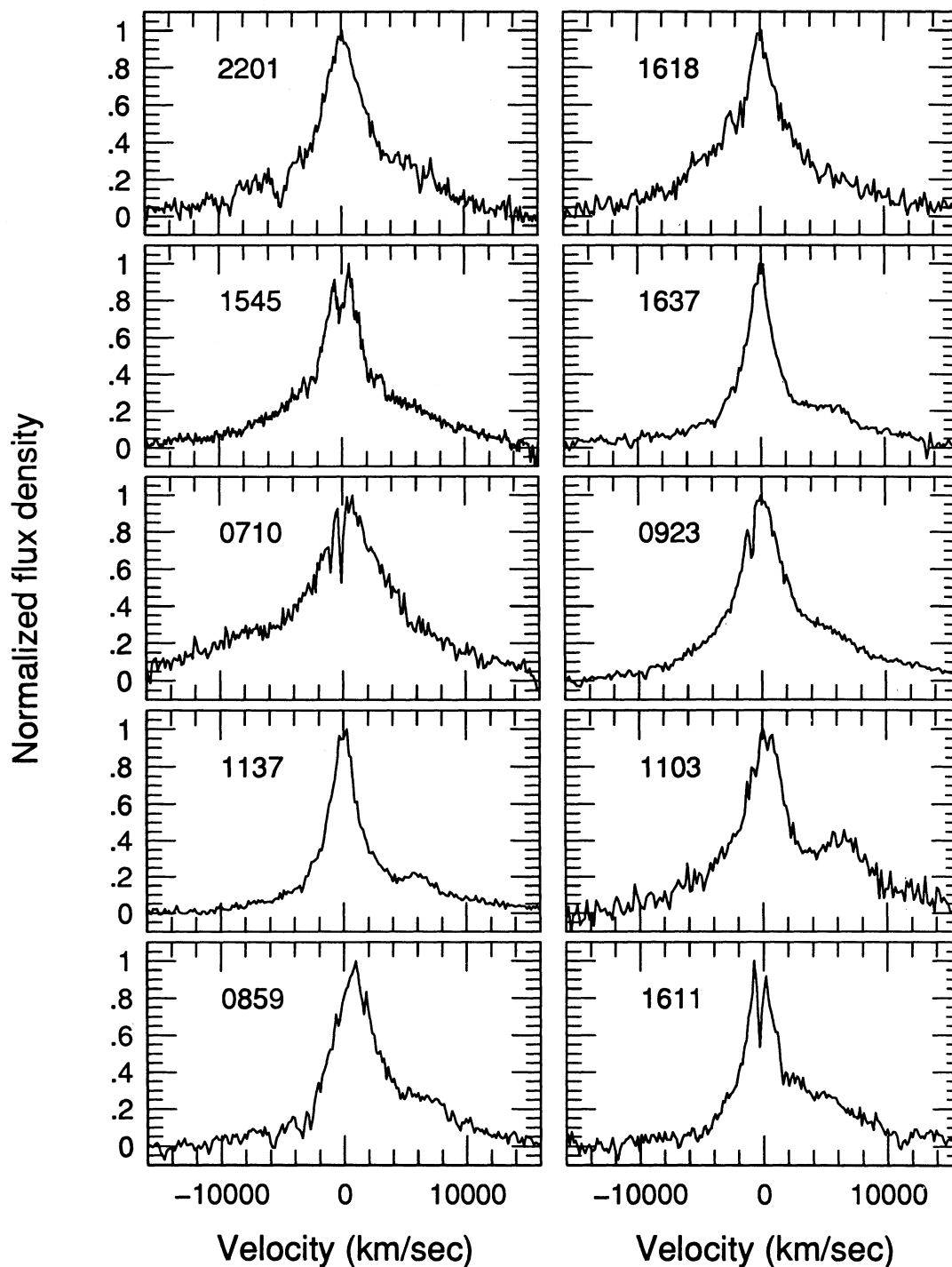


FIG. 1—Continued

with core component measured about the zero of velocity and including all flux within the FWHM of $\text{Ly}\alpha$, and the wings measured beyond the FWHM, at shorter and longer wavelengths from zero velocity. This division emphasizes the “typical” velocity field of individual sources.

3. Three components, a blue wing, a core, and a red wing, the core being defined by a 3000 km s^{-1} bin centered on zero velocity. The choice of bins of fixed velocity width is motivated by the successful description of line profiles in terms of cores of

identical width (e.g., Brotherton et al. 1994). Here, again, velocity is in the rest frame defined by the redshift of $[\text{O III}] \lambda 5007$.

The $\text{Ly}\alpha/\text{H}\beta$ ratios were measured for all the above individual components and are listed in Table 1 (the blue, core, and red line ratios are for using the $\text{Ly}\alpha$ FWHM as separation points). We also list the $\text{Ly}\alpha$ and $\text{H}\beta$ FWHMs and rest-frame equivalent widths (EW).

The above division into components involves some uncer-

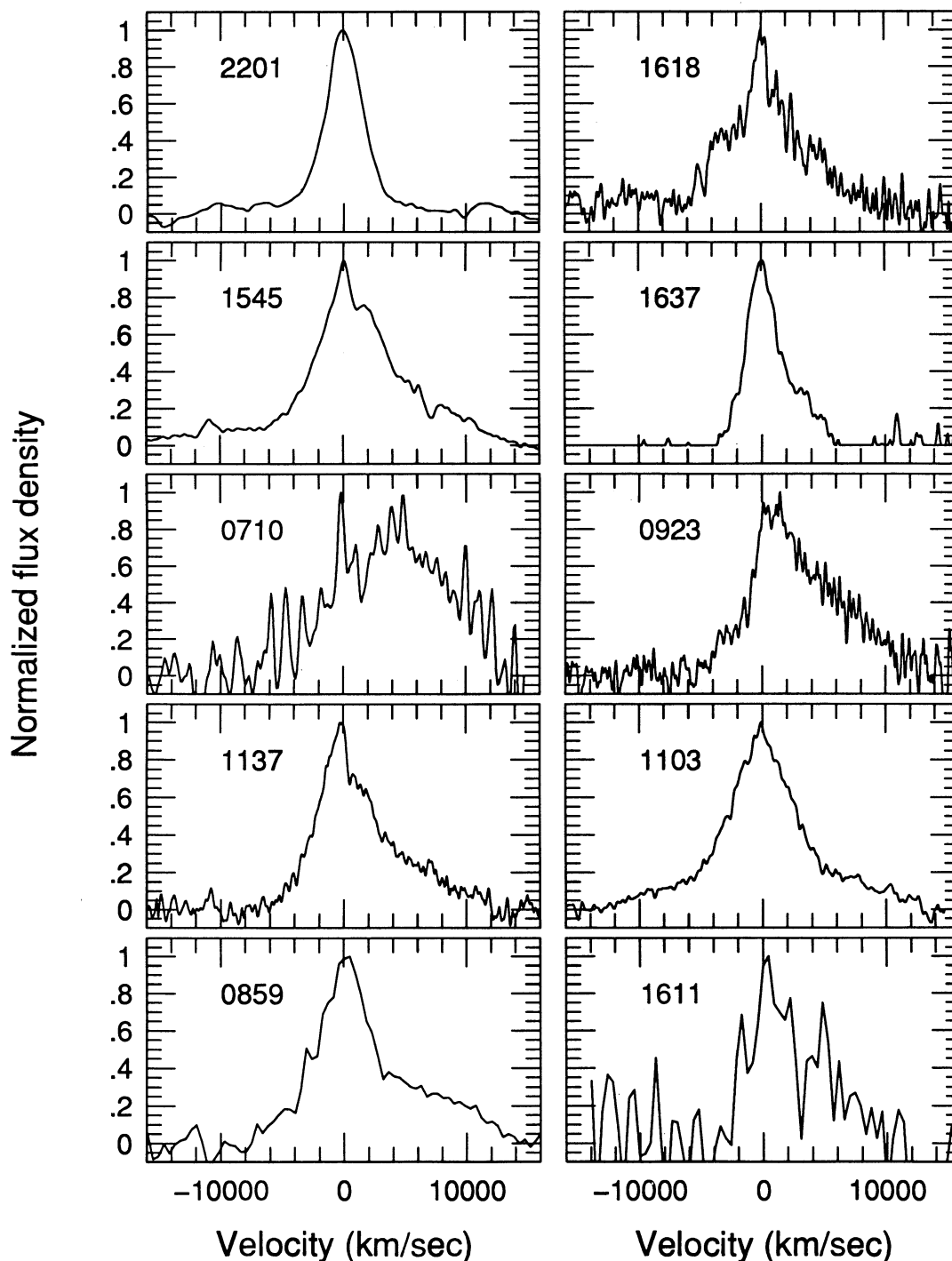


FIG. 2.—Continuum-subtracted, normalized $H\beta$ profiles for the 20 radio-loud quasars discussed in this work. Fe II blends and narrow [O III] lines have been removed as described in the text.

tainties, mostly in defining rest-frame wavelengths, in continuum placement, and in the deblending procedure. The blue wings of many $H\beta$ lines are rather weak, and the uncertainty in their measurements is particularly large. In addition, in many cases (Fig. 3), the $H\beta$ profile is shifted with respect to the Ly α profile so that the definition of a “line core” is not intuitive. It is not realistic to assign errors to individual line components, however; various tests show that the important line ratio

correlations discussed below are little affected by the exact definitions of FWHM, velocity width, or the exact wavelength dividing the profiles into red and blue wings.

Two-point spectral indices ($\alpha_{\lambda_1-\lambda_2}$, where λ is the rest wavelength and $F_\nu \propto \nu^{-\alpha}$) were defined over three wavelength ranges: 1215–1909, 1909–4861, and 1215–4861 Å. We have used the continuum flux density measurements at 1550 Å rest wavelength (slightly extrapolated, in one case) and *Einstein*

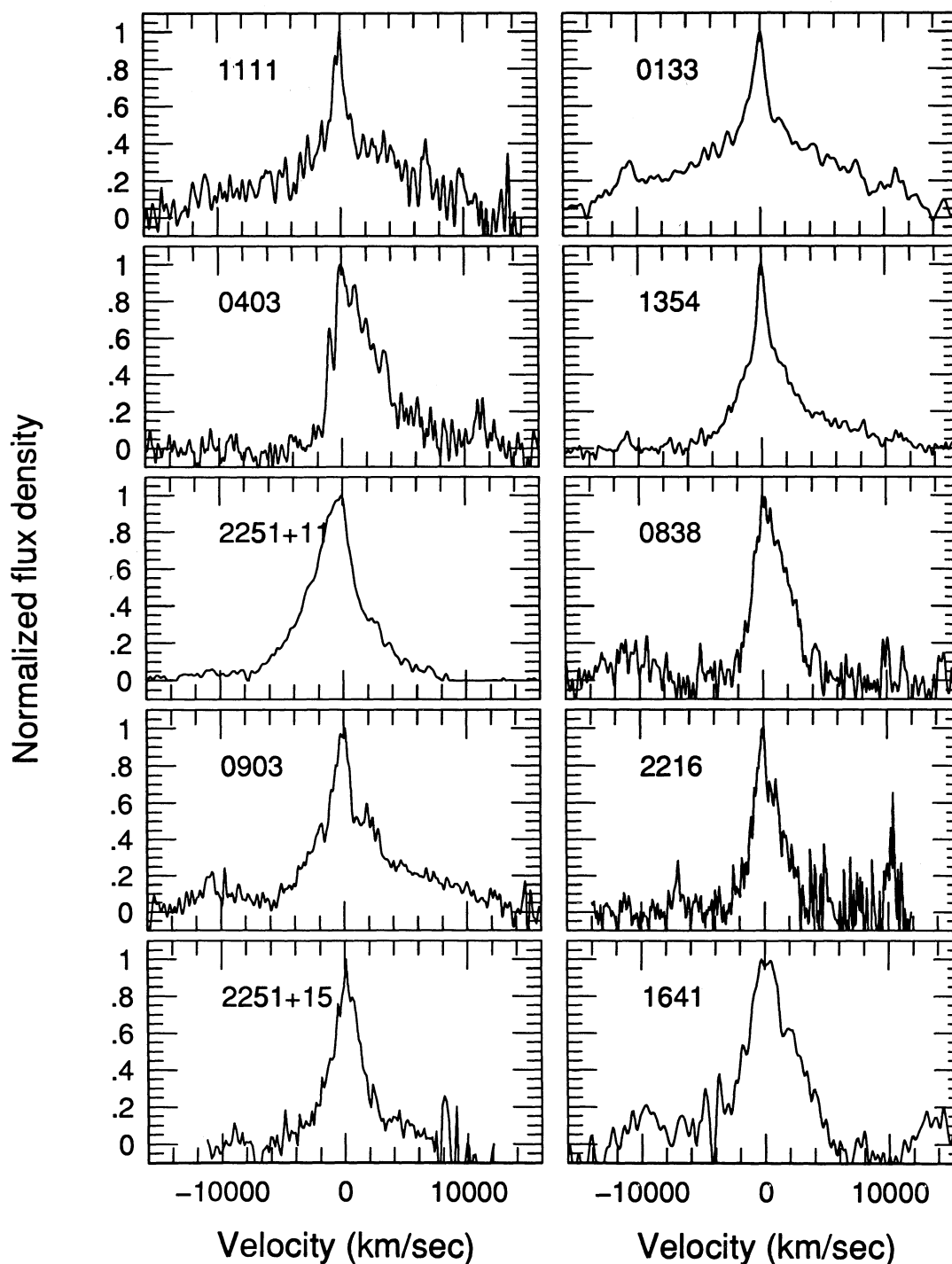


FIG. 2—Continued

X-ray measurements at a rest energy of 2 keV (Wilkes et al. 1994) to calculate α_{1550-X} . This spectral index is equivalent to the commonly used α_{ox} index (e.g., Kriss 1984) based on the 2500 Å continuum, but it is better defined because it avoids the strong Fe II blends near 2500 Å and because it uses a monochromatic rather than a broadband flux density. Comparison with values tabulated by Wilkes et al. (1994) shows very good agreement between α_{1550-X} and α_{ox} . The 2 keV measurements were obtained several years before our optical and UV spec-

troscopy, so α_{1550-X} would be affected by any variability of the optical and X-ray continuum.

3.2. New Ly α /H β Correlations

Standard correlation analysis was performed on all data shown in Table 1 and the other measured line parameters. Several significant correlations were found and are listed in Table 2 where we give the linear (Pearson's r) and Spearman's rank-order correlation coefficients, with their associated prob-

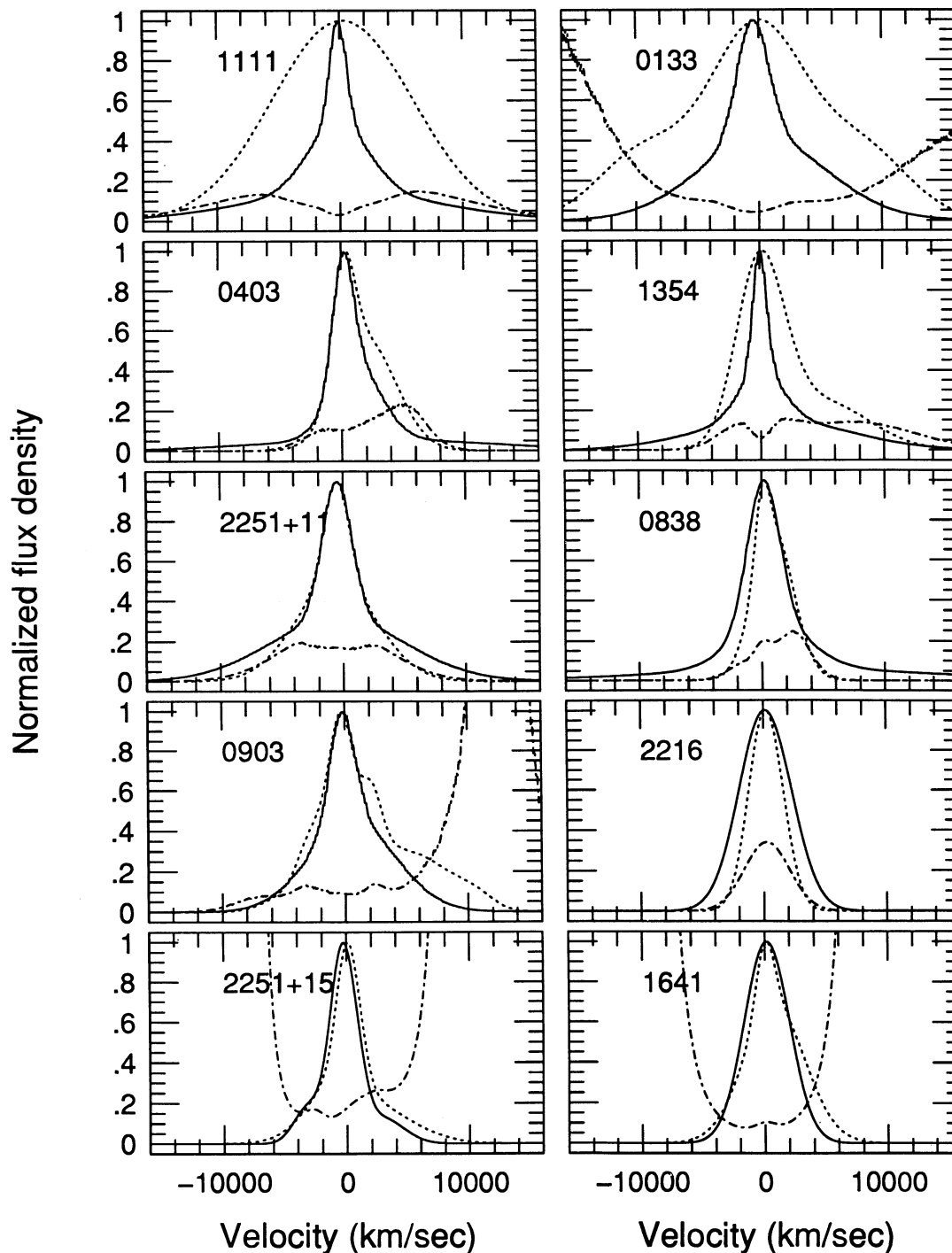


FIG. 3.—Observed, smoothed Ly α (solid line) and H β (dotted line) profiles for the 20 quasars. The objects are arranged in order of increasing continuum slope $\alpha_{4861-1215}$ (see text and Table 1). The profiles are normalized to unit peak intensity and the H β /Ly α ratio, as a function of velocity relative to the [O III] λ 5007 redshift, is shown as a dash-dotted curve. Objects are identified in the top left corner of each panel by the first four digits of the RA.

abilities (the two-tailed probability of the observed correlation arising by chance if the variables are uncorrelated). Listed in the table are correlations with probability of less than 1% in one of tests and no greater than 2% in the other test. Figure 4 shows several of the correlations that we consider most important. In all diagrams we identify radio lobe-dominated ($R < 1$) and core-dominated ($R > 1$) quasars by different symbols (see Table 1).

4. DISCUSSION

The data presented in this paper show the first significant correlations of the Ly α /H β ratio with other observed properties of quasars. The most interesting results are the new correlations of this ratio with various continuum slope indicators and the correlations involving line-profile components. Previous studies of the hydrogen line ratios (see Kriss 1984, 1986

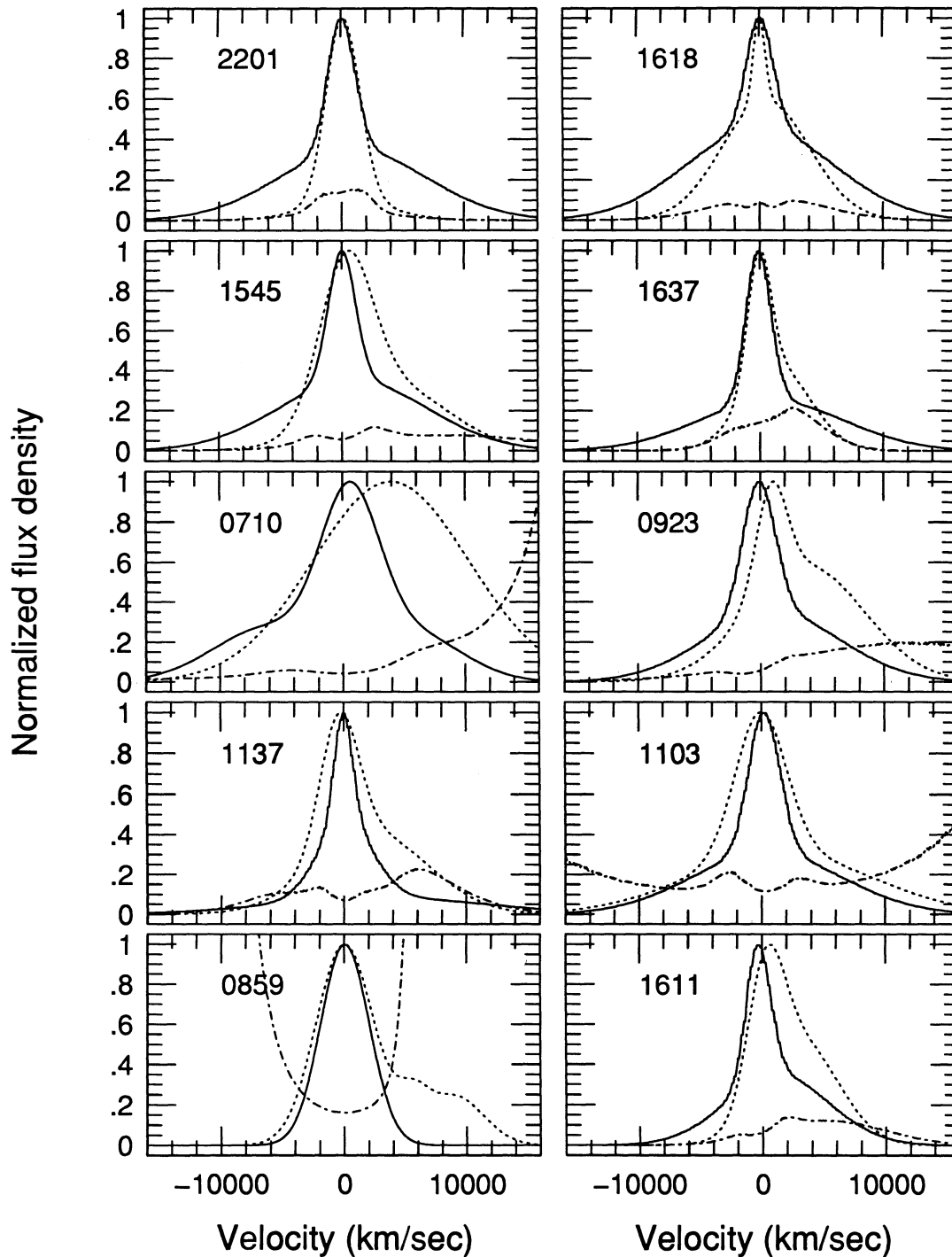


FIG. 3—Continued

for summaries) found no clear correlations with other properties. The only exception is the suggestion by Soifer et al. (1981) that the $\text{Ly}\alpha$ ratio is positively correlated with the continuum slope defined by the flux density ratio F_{1215}/F_{6563} . This trend, which is similar to one found here, was of no statistical significance.

Below we discuss the new results, first, by addressing the theoretical $\text{Ly}\alpha/\text{H}\beta$ ratio in AGNs and, second, by considering two possible explanations: reddening by external dust and a multiple-component continuum.

4.1. Theoretical $\text{Ly}\alpha/\text{H}\beta$ Ratios

The notable discrepancy between the observed and predicted $\text{Ly}\alpha/\text{H}\beta$ ratios in quasars stimulated detailed investigations of this and related problems of quasars' broad-line spectra. The intrinsic hydrogen line ratio depends on density and line optical depth in the BLR clouds. The fundamental difficulty with all BLR models is that they do not combine complete atomic treatment with accurate line transfer. The most comprehensive calculations so far (e.g., Kwan & Krolik 1981;

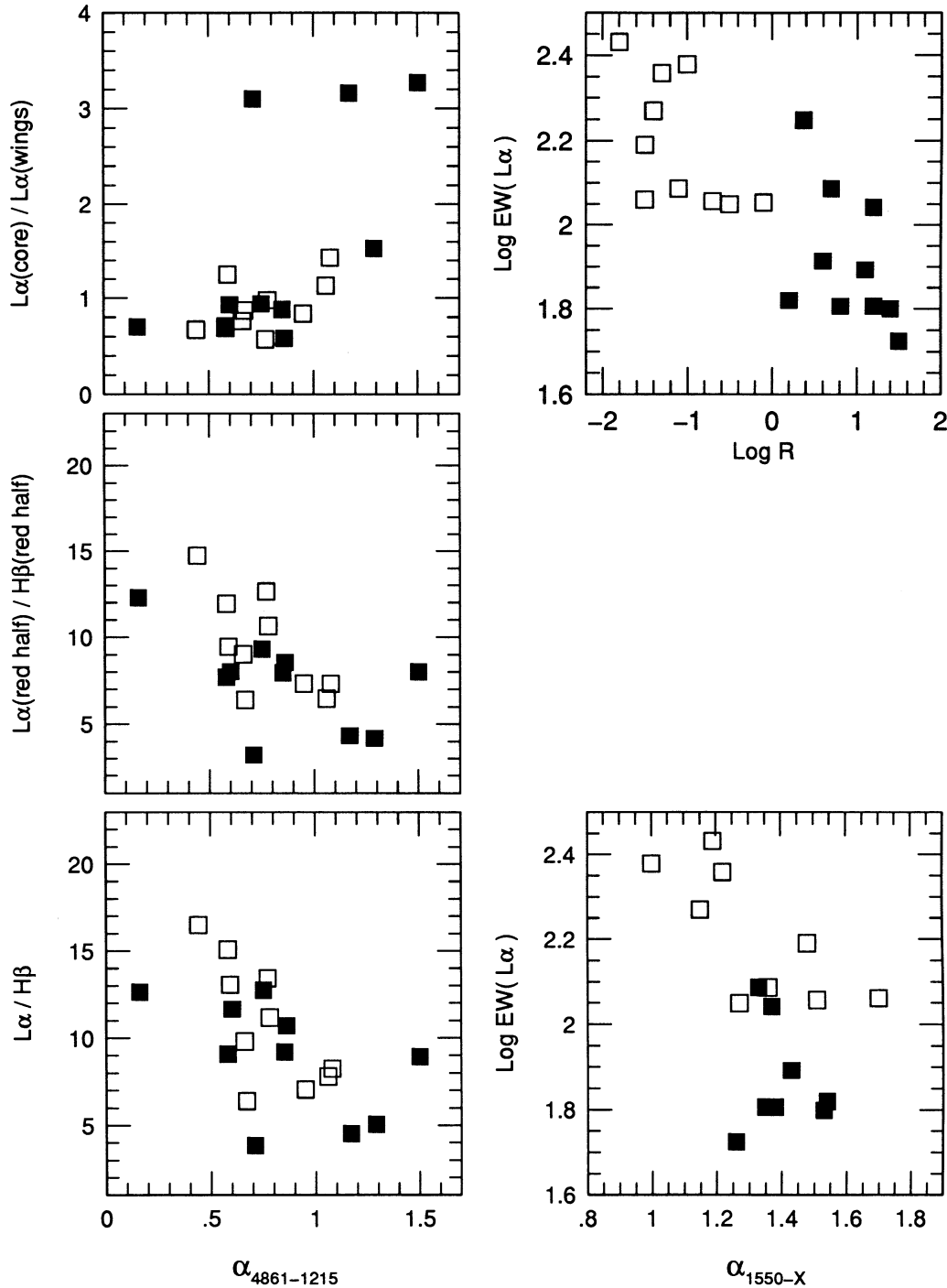


FIG. 4.—Several observed correlations in radio-loud quasars. Filled symbols in all diagrams indicate core-dominated sources with $R > 1$, and open squares indicate lobe-dominated sources with $R < 1$. For the levels of significance and more correlations, see Table 2.

Kwan 1984; Rees et al. 1989; Ferland & Persson 1989; Netzer 1993; Baldwin et al. 1995) are complete in their treatment of atomic processes but use a simple escape probability method for the evaluation of line transfer. The few models with better radiative transfer (e.g., Avrett & Loeser 1988; Hubbard & Puetter 1984; Collin-Souffrin et al. 1981) suffer in their treatment of the atomic processes, and their solution for the temperature and ionization structure is uncertain. This problem has been discussed by, e.g., Collin-Souffrin et al. (1981, 1986),

Collin-Souffrin & Dumont (1989), Rees et al. (1989), and Netzer (1990). While this fundamental difficulty is not yet resolved, we present here a grid of models, based on what we consider to be the most detailed calculations so far, to enable a comparison with the observations.

Figure 5 shows theoretical $\text{Ly}\alpha/\text{H}\beta$ ratios for a range of BLR conditions, calculated by G. Ferland's photoionization code CLOUDY (e.g., Baldwin et al. 1995). These results were compared with those of a second code, ION (Netzer 1993, and

TABLE 1
OBSERVED AND MEASURED PROPERTIES OF RADIO-LOUD QUASARS

OBJECT	z	log R	CONTINUUM SLOPE					Total	Ly α /H β				FWHM		REST EW	
			$\alpha_{4861-1909}$	$\alpha_{1909-1215}$	$\alpha_{4861-1215}$	α_{1550-x}	Blue Half		Red Half	Blue Wing	Core	Red Wing	Ly α	H β	Ly α	H β
0133+207.....	0.43	-1.0	0.74	0.86	0.78	1.00	11.2	11.7	10.6	7.4	19.3	8.4	4700	13500	239	117
0403-132.....	0.57	0.7	0.86	0.81	0.85	1.33	9.2	13.0	7.9	22.4	9.2	7.5	2800	4200	122	65
0710+118.....	0.77	-1.5	0.43	0.92	0.59	1.70	13.1	23.0	9.5	25.4	19.8	5.5	7300	15000	115	62
0838+133.....	0.68	-0.5	0.70	1.80	1.06	1.27	7.8	11.1	6.5	38.1	5.8	9.4	3800	3300	112	53
0859-140.....	1.33	0.8	0.77	0.59	0.71	1.38	3.9	5.0	3.2	3.6	5.8	1.4	4600	5700	64	100
0903+169.....	0.41	-1.4	1.28	0.66	1.08	1.15	8.2	9.8	7.3	8.1	11.8	4.8	3600	5200	186	79
0923+392.....	0.70	1.2	0.45	0.90	0.60	1.37	11.7	25.0	8.0	27.3	15.7	6.5	4200	7300	110	66
1103-006.....	0.43	-0.1	0.24	1.56	0.67	...	6.4	6.4	6.4	5.9	7.5	5.5	4100	6300	113	112
1111+408.....	0.73	-1.8	0.61	1.09	0.77	1.19	13.4	14.3	12.6	11.0	26.1	10.1	2700	13500	270	112
1137+660.....	0.65	-1.1	0.55	0.89	0.66	1.36	9.8	11.0	9.0	9.8	12.0	8.0	2800	5300	122	80
1354+195.....	0.26	0.4	0.58	1.44	0.86	...	10.7	14.7	8.6	14.4	13.7	7.5	2000	5200	177	80
1545+210.....	1.39	-1.3	0.49	0.77	0.58	1.22	15.1	21.9	11.9	29.4	14.6	11.4	3700	6300	228	108
1611+343.....	1.39	1.4	0.67	0.93	0.75	1.53	12.8	23.1	9.3	34.1	14.6	8.0	3200	5600	63	28
1618+177.....	0.56	-0.7	0.23	0.88	0.44	1.51	16.5	18.7	14.7	23.2	13.6	16.5	4200	4100	114	60
1637+574.....	0.75	0.6	0.40	0.94	0.58	...	9.1	11.4	7.7	18.9	7.2	8.4	2800	3200	82	65
1641+399.....	0.59	1.5	1.44	1.61	1.50	1.26	8.9	10.3	8.0	8.0	10.5	5.1	4400	4200	53	12
2201+315.....	0.30	0.2	-0.16	0.82	0.16	1.54	12.6	13.0	12.3	28.6	7.1	26.5	3700	3400	66	67
2216-038.....	0.90	1.1	0.97	1.58	1.17	1.43	4.5	4.8	4.3	18.2	3.7	12.4	5000	3300	78	55
2251+113.....	0.32	-1.5	0.95	0.97	0.95	1.48	7.1	6.9	7.3	7.8	5.9	9.5	3800	3800	155	94
2251+158.....	0.86	1.2	1.10	1.68	1.29	1.35	5.1	6.2	4.2	5.7	5.7	3.3	2800	2800	64	34

TABLE 2
CORRELATION COEFFICIENTS AND PROBABILITIES FOR VARIOUS MEASURE PROPERTIES

VARIABLE a	VARIABLE b	n	PEARSON'S r		SPEARMAN RANK-ORDER	
			r	Probability	r	Probability
$\alpha_{4861-1909}$	Ly α /H β	20	-0.51	0.020	-0.57	0.008
$\alpha_{4861-1909}$	Ly α (core/wing)	20	0.59	0.006	0.66	0.001
$\alpha_{4861-1909}$	Ly α /H β (3000 red)	20	-0.65	0.002	-0.52	0.018
$\alpha_{4861-1215}$	Ly α /H β	20	-0.58	0.008	-0.62	0.004
$\alpha_{4861-1215}$	Ly α /H β (red half)	20	-0.58	0.008	-0.58	0.008
$\alpha_{4861-1215}$	Ly α (core/wing)	20	0.59	0.006	0.59	0.007
$\alpha_{4861-1215}$	Ly α /H β (3000 red)	20	-0.64	0.002	-0.55	0.012
α_{1550-X}	L(Ly α)	17	0.63	0.007	0.74	<0.001
α_{1550-X}	L ₁₂₁₅	17	0.61	0.009	0.77	<0.001
Ly α /H β	Ly α (core/wing)	20	-0.60	0.005	-0.62	0.004
Ly α /H β	C IV/H β	19	0.61	0.005	0.59	0.008
Ly α /H β (red half)	Ly α (core/wing)	20	-0.60	0.005	-0.64	0.002
Ly α /H β (red half)	C IV/H β	19	0.59	0.007	0.58	0.009
Ly α /H β (core)	H β (FWHM)	20	0.84	<0.001	0.79	<0.001
Ly α /H β (core)	EW(Ly α)	20	0.66	0.001	0.54	0.014
Ly α /H β (3000 core)	H β (FWHM)	20	0.89	<0.001	0.81	<0.001
EW(Ly α)	log R	20	-0.74	<0.001	-0.82	<0.001
EW(Ly α)	L ₁₂₁₅	20	-0.60	0.005	-0.62	0.004
EW(H β)	log R	20	-0.63	0.003	-0.60	0.005
C IV/H β	L(H β)	19	-0.60	0.007	-0.59	0.008

references therein). The two codes give similar solutions to the line ratio, given the same escape probability approximation. The figure shows the Ly α /H β ratio predicted for a series of calculations with fixed continuum shape, similar to that deduced by Mathews & Ferland (1987), and solar chemical composition. Constant hydrogen density, n_H , across a cloud was assumed, and the flux of ionizing photons $\Phi(H)$ (photon $s^{-1} cm^{-2}$) varied over a wide range of values. These results are from the grid of BLR models generated by Baldwin et al. (1995). We show results as a function of the ionizing photon flux and the hydrogen density rather than as their ratio, the ionization parameter U , since $\Phi(H)$ is conveniently proportional to the inverse square of the source-cloud separation [the conventional ionization parameter of $10^{-1.5}$ corresponds to $\Phi(H)/n_H = 10^9 cm s^{-1}$]. All clouds are radiation bounded, i.e., have sufficient column density to nearly fully absorb the incident continuum.

Several trends are evident. Points are not plotted at the high-flux, low-density corner of the diagram since these correspond to ionization parameters so large that the gas is in equi-

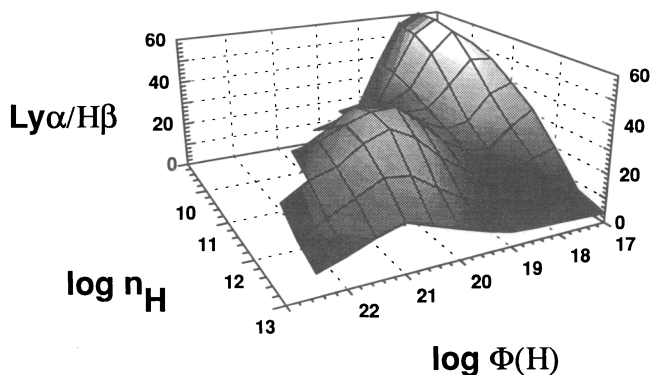


FIG. 5.—Calculated Ly α /H β ratios for a grid of constant density models, as a function of the hydrogen density n_H and incident photon flux $\Phi(H)$ (photons $cm^{-2} s^{-1}$). For explanation see text.

librium at the Compton temperature of the continuum source rather than at nebular temperatures. Such clouds would effectively be spectroscopically invisible. For parameters with nebular solutions we see that the largest ratios are found for lower densities and fluxes. Collisional excitation of Ly α can rise the Ly α /H β ratio well above that (35) expected for pure recombination. Denser clouds, where collisional suppression of level 2 is important, tend to have smaller Ly α /H β ratios. For expected BLR fluxes $\Phi(H)$, the line ratio, is mostly in the range 20–30. It is important to note that Ly α /H β ratios of order unity are not predicted, yet such ratios are observed in the wings of the lines of some objects (see Fig. 3).

Figure 5 presents the results of this particular model just as an example because basic questions remain about the shape of the continuum striking the clouds, their composition and equation of state, the formation of hydrogen lines under these conditions, and whether all clouds contributing to the net spectrum are optically thick. The model calculations do point to some possible causes of the core-wing distinction evident in Figure 3 and Table 2. For instance, the observed line profiles could be modeled as a core with larger Ly α /H β ratio and wings with smaller Ly α /H β ratio. If the wings are formed at smaller radius (higher flux) than the core, then the fact that the wings have a shallower decrement limits parameters to only certain regions. These results are the basis for the following comparison with the observations.

4.2. External Reddening

There are two indications that external reddening may be important. The extreme Ly α /H β ratios of order unity in the red wings of the lines of some objects are not consistent with photoionization models. And the correlations of the Ly α /H β ratio with the various continuum slopes suggest that the broad emission lines and the nonstellar continuum may be subjected to extinction by dust (a “dust screen”) located outside the BLR and the continuum source. Reddening by such dust steepens the intrinsic continuum and decreases the intrinsic Ly α /H β correspondingly.

Reddening of quasars' broad emission lines has been suggested, on theoretical grounds, by Netzer & Davidson (1979) and has been discussed in many papers since. This idea followed the failure of other explanations of the observed hydrogen line ratios and was claimed to improve the agreement between the observed and predicted intensity ratios of other lines. The line reddening was required even after including the effects of high density and high optical depth. It was suggested that continuum reddening might also be present but not necessarily equal to that of the lines. In a later paper, De Zotti & Gaskell (1985) argued that the broad Balmer line ratios in AGNs are correlated with the axial ratio of the host galaxy and interpreted this as due to reddening by dust in the disk of the galaxy. Much more recently it has been appreciated that dust absorption and emission is a key ingredient in various unified schemes for luminous AGNs to the extent of completely determining the AGNs' classification (e.g., Hines & Wills 1993; see also earlier discussion by Rowan-Robinson 1977).

As argued by Netzer & Davidson (1979), there are two line ratios that are particularly suitable as reddening indicators: $[\text{O I}] \lambda 8446/[\text{O I}] \lambda 1304$ and $\text{He II } \lambda 4686/\text{He II } \lambda 1640$. Note, however, that the usefulness of these was challenged in several papers (e.g., Grandi 1983) on the grounds that optical depth effects can influence the line ratios. Unfortunately, neither can be used in the present study. $[\text{O I}] \lambda 8446$ is not observed in our sample, and $[\text{O I}] \lambda 1304$ is extremely weak. The $\text{He II } \lambda 4686$ line is present in about one-fourth of the objects, but is weak and blended with the blue wing of $\text{H}\beta$ and the strong Fe II lines, which precludes reliable intensity measurements. $\text{He II } \lambda 1640$ is also blended. We cannot even use the Balmer decrement; we do not have $\text{H}\alpha$ measurements for most of the objects, and $\text{H}\gamma$ is too weak and blended to be measured reliably in most cases. So we must rely on correlations with continuum and other properties.

We have analyzed the correlation of the $\text{Ly}\alpha/\text{H}\beta$ ratios with the three UV-optical spectral indices (Table 1) to test for reddening. We assume that the intrinsic continuum shape is the same in all objects. In this case we expect a gradual change in slope, with more extinction at shorter wavelengths. In 17 out of 20 objects studies here, $\alpha_{1909-1215}$ is indeed greater than $\alpha_{4861-1909}$. However, we find no significant correlation between the $\text{Ly}\alpha/\text{H}\beta$ ratio and the difference between $\alpha_{1909-1215}$ and $\alpha_{4861-1909}$. As noted earlier, the short-wavelength continuum is curved in many cases, and its description by a single slope between 1909 and 1215 Å is too simple. Moreover, in tests carried out with a different short-wavelength continuum slope, defined by a least-square fit to the data, we found some correlations that are not seen for the two-point spectral index $\alpha_{1909-1215}$. In § 4.3 we discuss possible explanations for the $\text{Ly}\alpha/\text{H}\beta$ versus slope correlations in terms of several continuum components.

To further check for consistency, we examined the actual relation between the $\text{Ly}\alpha/\text{H}\beta$ ratio and F_{1215}/F_{4861} and found that it was consistent with a proportional relationship as expected for an external reddening screen. In Figure 6 we show a reddening line with values of E_{B-V} calculated assuming intrinsic ratios of $\text{Ly}\alpha/\text{H}\beta = 20$ and $F_{1215}/F_{4861} = 10$ ($\alpha_{4861-1215} = 0.34$) and a Galactic extinction law. The data are consistent with reddenings up to $E_{B-V} = 0.3$. Interestingly, this and larger reddenings would correspond to colors too red to select quasars by commonly used methods (e.g., for the PG survey, or by comparison of prints of the National Geographic-Palomar Observatory Sky Survey).

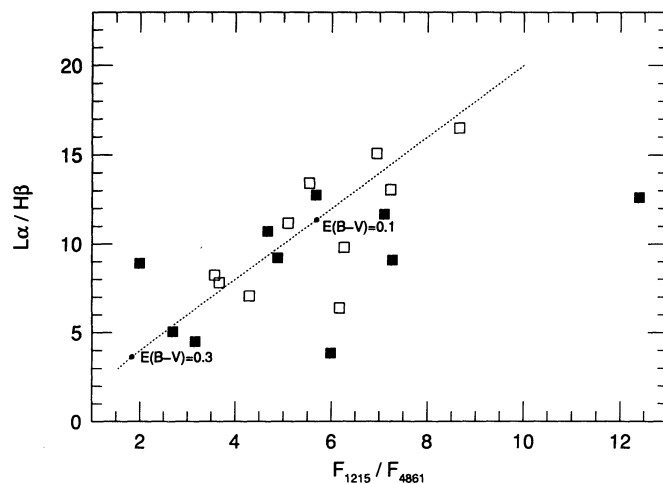


FIG. 6.—Galactic extinction curve, with specified values of E_{B-V} (dashed line), is compared with the observed correlation of the $\text{Ly}\alpha/\text{H}\beta$ ratio and the continuum flux density ratio F_{1215}/F_{4861} .

Finally, for the simple reddening explanation, we expect a correlation between the observed $\text{C IV } \lambda 1549/\text{H}\beta$ ratio and the continuum shape. We find weak, insignificant correlations for all continuum indices. This test is inconclusive in the presence of intrinsic scatter, because the effect of reddening is expected to be smaller at $\text{C IV } \lambda 1549$ than at $\text{Ly}\alpha$.

It is of interest to relate the possible line and continuum reddening to the special nature of the radio sample under discussion. In the Unification Scheme for radio sources (e.g., Orr & Browne 1982; Barthel 1989), core-dominated sources are those where our line of sight is at a small angle to the radio beam, while the lobe-dominated one are at large angles. If the ionized gas clouds lie in a plane perpendicular to the beam, the lobe-dominated sources are the objects where we might expect absorbing gas and dust along the line of sight to both the emission-line and continuum regions. This idea can be examined since the radio core-to-lobe luminosity ratio R is known. We have tested the various line and continuum ratios and found no significant correlations between the core dominance, R , and any of the possible reddening indicators such as the $\text{Ly}\alpha/\text{H}\beta$ ratio, F_{1215}/F_{4861} , etc. The R versus F_{1215}/F_{4861} correlation is even present in the wrong sense in our larger sample (or Paper II) and other samples; it is clear that the simple model involving orientation and reddening in the plane perpendicular to the radio jet cannot explain the correlations found in the present data set.

Another test involving radio properties is to check whether the observed correlations arise from the core-dominated or lobe-dominated sources. In the present sample there are 10 of each subgroup and while, numerically, there is a significant correlation of $\text{Ly}\alpha/\text{H}\beta$ with slope for the lobe-dominant quasars alone (at a level of $\leq 1.5\%$), the difference between the subgroups is insignificant.

4.3. A Multicomponent Continuum

Our sample of radio-loud objects differs from radio-quiet samples in including some sources with steep optical-UV continua, in particular 2251 + 158 (3C 454.3) and 1641 + 399 (3C 345), and perhaps others. Polarimetry and variability studies show the presence of a radio-IR synchrotron source extending into the optical and UV regions, in addition to the usual

quasar continuum. The typical slope of such a component is ~ 2 , as indicated by the recent 3C 279 observations by Netzer et al. (1994) and the very steep polarized flux spectra of many blazars (Wills 1990). This component differs in shape from the typical continuum slope of ~ 0.7 of most radio-quiet objects (e.g., Laor 1990), thought to arise from thermal emission, e.g., an accretion disk. The steep synchrotron component in core-dominated objects is added to the disk component, in various proportions, to give steeper spectra, especially at longer wavelengths. In our sample the shorter wavelength continuum is steeper, in most cases, than the long-wavelength part, suggesting that if accretion disks are important, we may be looking at the short-wavelength decline of the thermal emission of the disk (see Laor & Netzer 1989).

The presence of different amounts of synchrotron continuum is probably at least one cause of the decrease in $\text{EW}([\text{O III}] \lambda 5007)$ with increasing R in radio-loud quasars (e.g., Wills & Browne 1986; Jackson et al. 1987). We suspect that the strong negative correlation we find between $\log R$ and $\log \text{EW}(\text{Ly}\alpha)$ (Fig. 4) is of similar origin. This could be caused by a combination of a narrow-angle beamed continuum and a spherical gas distribution whose line emission is only weakly affected by the beam radiation. As noted earlier, lobe-dominated objects, with negligible synchrotron components, seem to be the drivers of the $\text{Ly}\alpha/\text{H}\beta$ continuum shape correlations. Even in the core-dominant sources of this sample, the synchrotron component is expected to be weak at 1216 Å. Thus the synchrotron continuum component suggested as the cause of the small $\text{EW}(\text{Ly}\alpha)$ cannot be the steep continuum related to the small $\text{Ly}\alpha/\text{H}\beta$ ratio.

We are left with the possibility that the intrinsic ionizing continuum differs in shape from one source to the next, resulting in different ionizing flux and line strengths. We note that this explanation is in conflict with the simplest unified scheme where it is assumed that the intrinsic spectrum of quasars is identical except for the orientation-dependent synchrotron continuum.

Accepting the dependence of the $\text{Ly}\alpha/\text{H}\beta$ ratio on ionizing continuum shape, it is of interest to examine whether the observed decrease in $\text{Ly}\alpha/\text{H}\beta$ with increasing continuum slope is the result of a decrease in $\text{Ly}\alpha$ flux, an increase in $\text{H}\beta$, or, perhaps, both. For example, the $\text{Ly}\alpha$ flux may be closely related to the soft (a few rydberg) ionizing continuum, while $\text{H}\beta$ may be more sensitive to the higher energy radiation. Such an explanation requires that the 1–5 ryd continuum flux decreases with increasing continuum slope while the harder ionizing continuum (for which we have no direct information) may be less affected. In the present sample there is no significant correlation of $\text{EW}(\text{Ly}\alpha)$ with any optical-UV continuum slope, as would be expected if the $\text{Ly}\alpha$ line is affected by soft-continuum steepening. There is also no significant correlation of $\text{EW}(\text{H}\beta)$ with those slopes, suggesting that the explanation may involve a change of more than one parameter. We note, however, that $\text{EW}(\text{H}\beta)$ may be affected by the continuum slope in another way, because of the increased F_{4861} in steep synchrotron continuum cases. To overcome this complication we have calculated a modified $\text{EW}(\text{H}\beta)$, taking the ratio of the observed $\text{H}\beta$ flux and the 1215 Å continuum. No significant correlation with continuum slope was found. The only suggested correlation of any slope with line equivalent width is of $\text{EW}(\text{Ly}\alpha)$ with α_{1550-x} . Using the Pearson's r coefficient, this correlation is strong, but it is marginal (4%) when Spearman's rank-order correlation coefficient is used. The correlation for

$\text{EW}(\text{H}\beta)$ is even weaker, and more data are required to confirm this, especially for core-dominated sources (Fig. 4, *bottom right panel*). If real, it is not possible to tell whether the $\text{Ly}\alpha$ luminosity or the 1215 Å continuum luminosity causes this, since both are correlated with α_{1550-x} .

Finally, much of the dependence of $\text{H}\beta/\text{Ly}\alpha$ with continuum slope may be the result of ionization by the Balmer continuum is very thick BLR clouds, since steeper continua correspond to larger Balmer flux. In this case, much of the additional Balmer ionization results in Balmer line production, as the $\text{Ly}\alpha$ optical depth in the partially ionized zones is extremely large. This would predict a stronger $\text{H}\beta$ luminosity for a given continuum luminosity.

In summary, our data, while showing clear correlations of the $\text{Ly}\alpha/\text{H}\beta$ ratio with various continuum shapes, still do not provide enough information to establish a clear and unique explanation. Reddening seems to explain most correlations but we suspect that the real situation is rather complex, involving various other processes.

4.4. Core-Wing Correlations

An interesting finding of the present study is the strong correlation of different line components with the total $\text{Ly}\alpha/\text{H}\beta$ ratio and the various continuum indices. Most of the strong $\text{Ly}\alpha/\text{H}\beta$ ratio correlations involve the red wings of the lines. The line ratio in the blue wing is not correlated with slope, and the core's $\text{Ly}\alpha/\text{H}\beta$ correlation is marginal or absent. The general trend is for $\text{H}\beta$ to be relatively stronger at larger velocities from the line center for those objects with the steeper continua. The most extreme $\text{Ly}\alpha/\text{H}\beta$ ratio, in the far red wing of some lines, is less than 1. While we are not sure of the exact value, because of the uncertainty in subtraction of the N v $\lambda 1240$ line, the trend from blue to red must be real. As for the $\text{Ly}\alpha(\text{core})/\text{Ly}\alpha(\text{wing})$ correlation with slope (Fig. 4), we find this to arise from core-dominated sources and to be correlated most strongly with the 4861–1909 Å continuum. This correlation is influenced by three extreme cases and their removal considerably reduces its significance.

It is not our intention here to develop a consistent model for the gas motions and line profiles. We only comment that the red wings of the lines appear to have the smallest $\text{Ly}\alpha/\text{H}\beta$ ratio. On the external reddening hypothesis, these wings would come from a region subjected to the largest amount of reddening. This would be consistent with an outflow of the BLR gas in a dusty medium of large filling factor, assuming individual clouds emit isotropically. This idea does not fully explain the relative velocity shift between the line centers, and there are complications with the assumption of isotropic emission by the clouds. An alternative that was discussed in the literature (e.g., Kallman et al. 1993; Ferland et al. 1992), and which does not require any dust, is a line emission asymmetry caused by a different optical depth structure of $\text{H}\beta$ and $\text{Ly}\alpha$. In most BLR photoionization models, the $\text{Ly}\alpha$ emission is highly non-isotropic because of the ionization structure within the clouds. However, the largest opacity for the Balmer lines is in the partially ionized region at the back of the clouds, and this opacity can vary across the BLR. This can cause location-dependent back-to-front emission asymmetry of the Balmer lines since most of the line photons escape from the illuminated side of the clouds. The location of clouds with such extreme conditions depends on the radial change of ionization parameters, density, and column density. We have not investigated this scenario mainly because of the large uncertainty associ-

ated with the escape probability formalism in extreme, nonuniform optical depth conditions.

5. CONCLUSIONS

We have observed a sample of radio-loud quasars with *HST* and several ground-based telescopes and found the first significant correlations between the $Ly\alpha/H\beta$ ratio and other properties. The strongest correlations are with various continuum slope indicators. In particular, the $Ly\alpha/H\beta$ ratio is weaker in steeper continuum sources. Several possible explanations were discussed. Reddening by an external dust screen is consistent with the observed properties, but dependences on ionizing photon flux may be important too. The correlations are nominally stronger in lobe-dominated quasars and probably arise in the red wings of the hydrogen lines. This may indicate

partial obscuration by dust or asymmetric line emission. Much stronger tests of the ideas presented in this paper will be possible when the complete sample of spectra for ~ 50 quasars is in hand.

It is a pleasure to acknowledge the support of the technical staffs of McDonald Observatory, CTIO, KPNO, and UKIRT. We thank the Space Telescope Science Institute (STScI) for support under grant HST GO-2578.01-87A RQ-Q. STScI is operated by AURA, Inc., under NASA contract NAS 5-2655. This research is also supported by the US-Israel Binational Science Foundation grant 8900179. G. J. F. thanks the NSF for support through grant AST 93-19034 and NASA through grant NAGW 3315.

REFERENCES

- Allen, D., Barton, J., Gillingham, P. R., & Carswell, R. F. 1982, *MNRAS*, 200, 271
- Avrett, E. H., & Loeser, R. 1988, *ApJ*, 331, 211
- Baldwin, J. A. 1977, *MNRAS*, 178, 67p
- Baldwin, J. A., Ferland, G. J., Hamann, F., Carswell, R. F., Phillips, M. M., Wilkes, B. J., & Williams, R. E. 1995, in preparation
- Barthel, P. D. 1989, *ApJ*, 336, 606
- Boroson, T. A., & Green, R. F. 1992, *ApJS*, 80, 109
- Brotherton, M. S. 1995, *ApJ*, submitted
- Brotherton, M. S., Wills, B. J., Francis, P. J., & Steidel C. C. 1994, *ApJ*, 430, 495
- Canfield, R. C., & Puetter, R. C. 1981, *ApJ*, 243, 390
- Collin-Souffrin, S., Delache, P., Dumont, A. M., & Frische, H. 1981, *A&A*, 104, 264
- Collin-Souffrin, S., & Dumont, A. M. 1989, *A&A*, 213, 29
- Collin-Souffrin, S., Dumont, A. M., Joly, M., & Pequignot, D. 1986, *A&A*, 166, 27
- De Zotti, G., & Gaskell, C. M. 1985, *A&A*, 147, 1
- Ferland, G. J., & Mushotzky, R. F. 1984, *ApJ*, 286, 42
- Ferland, G. J., & Persson, S. E. 1989, *ApJ*, 347, 656
- Ferland, G. J., Peterson, B. M., Horne, K., Welsh, W. F., & Nahar, S. N. 1992, *ApJ*, 387, 95
- Grandi, S. 1983, *ApJ*, 268, 591
- Hines, D. C., & Wills, B. J. 1993, *ApJ*, 415, 82
- Hubbard, E., & Puetter, R. C. 1984, *ApJ*, 290, 394
- Jackson, N. J., Browne, I. W. A., Murphey, D. W., & Saikia, D. J. 1987, *Nature*, 338, 485
- Kallman, T. R., & Krolik, J. H. 1986, *ApJ*, 308, 805
- Kallman, T. R., Wilkes, B. J., Krolik, J. H., & Green, R. 1993, *ApJ*, 403, 45
- Kriss, G. A. 1984, *ApJ*, 277, 495
- . 1986, *AJ*, 90, 1
- Kwan, J. 1984, *ApJ*, 283, 70
- . 1986, *ApJ*, 305, 679
- Kwan, J., & Krolik, J. H. 1981, *ApJ*, 250, 478
- Laor, A. 1990, *MNRAS*, 246, 369
- Laor, A., & Netzer, H. 1989, *MNRAS*, 238, 897
- Mathews, W. G., & Ferland, G. J. 1987, *ApJ*, 323, 456
- Netzer, H. 1990, in *Active Galactic Nuclei*, ed. R. D. Blandford, H. Netzer, & L. Woltjer (Berlin: Springer), 57
- . 1993, *ApJ*, 411, 594
- Netzer, H., & Davidson, K. 1979, *MNRAS*, 187, 871
- Netzer, H., Kazanas, D., Wills, B. J., Wills, D., Han, M., Brotherton, M. S., Baldwin, J. A., Ferland, G. J., & Browne, I. W. A. 1994, *ApJ*, 430, 191
- Orr, M. J. L., & Browne, I. W. A. 1982, *MNRAS*, 200, 1067
- Puetter, R. C., Smith, H. E., Willner, S. P., & Pipher, J. C. 1981, *ApJ*, 243, 345
- Rees, M., Netzer, H., & Ferland, G. J. 1989, *ApJ*, 347, 640
- Rowan-Robinson, M. 1977, *ApJ*, 213, 635
- Soifer, B. T., Neugebauer, G., Oke, J. B., & Matthews, K. 1981, *ApJ*, 243, 369
- Weisheit, J. C., Shields, G. A., & Tarter, C. B. 1981, *ApJ*, 245, 406
- Wilkes, B. J., Tananbaum, H., Worrall, D. M., Avni, Y., Oey, M. S., & Flanagan, J. 1994, *ApJS*, 92, 53
- Wills, B. J. 1990, in *Variability of Active Galactic Nuclei*, ed. H. R. Miller & P. J. Wiita (Cambridge: Cambridge Univ. Press), 87
- Wills, B. J., & Browne, I. W. A. 1986, *ApJ*, 302, 56
- Wills, B. J., Han, M., Netzer, H., Wills, D., Baldwin, J. A., Ferland, G. J., Browne, I. W. A., & Brotherton, M. S. 1995a, *ApJ*, in press (Paper II)
- Wills, B. J., Netzer, H., Brotherton, M. S., Han, M., Wills, D., Baldwin, J. A., Ferland, G. J., & Browne, I. W. A. 1993, *ApJ*, 410, 534 (Paper I)
- Wills, B. J., Netzer, H., & Wills, D. 1985, *ApJ*, 288, 94
- Wills, B. J., et al. 1995b, in preparation
- Wu, C. C., Boggess, A., & Gull, T. R. 1983, *ApJ*, 266, 28